Dilute Magnetic III-N Semiconductors Based on Rare Earth Doping

J. K. Hite [1,*] **and J. M. Zavada** [2,*,z]

[1] *U. S. Naval Research Laboratory, Washington, DC, 20375 USA*
[2] *Tandon School of Engineering, New York University, New York 11201, USA*

This paper focuses on the magnetic properties of wide bandgap III-N semiconductors doped with rare earth elements. Such materials form a novel class of dilute magnetic semiconductors that have an important potential impact on future information processing devices. In particular, rare earth doped III-N thin films may lead to integration of electronic, optical, and magnetic functionality for computation, sensing, and communication applications. The main aspects of this paper concern the efficient incorporation of rare earth ions in III-N thin films and the demonstration of magnetic effects at room temperature. While early studies were based on ion implantation and solid-state diffusion, major advances have been achieved through molecular beam epitaxy and metal-organic chemical vapor deposition. Measurements of room temperature magnetic effects from III-N films doped with rare earth elements, including erbium, gadolinium, europium, neodymium, and thulium, are presented. The dependence of measured magnetic properties on the synthesis method, co-doping, and material defects are addressed.

 [DOI: 10.1149/2.0261909jss]

Manuscript submitted July 22, 2019; revised manuscript received August 22, 2019. Published September 6, 2019.

The group III-Nitride (III-N) semiconductors constitute one of the most important material systems to be developed in the past 50 years.[1] This material system includes the binary compounds InN, GaN, and AlN as well as their ternary and quaternary alloys. These crystalline compounds are direct bandgap semiconductors that have a bandgap energy (*E*g) ranging from 0.7 eV for InN to 3.42 eV for GaN and 6.2 eV for AlN. The large *E*g range and the direct bandgap nature have made these materials attractive for optoelectronic devices. While these compounds typically form a wurtzite crystal lattice, cubic structures are also possible. In general, as *E*g increases, the bond length in the crystal lattice decreases. The large bonding energy of these materials requires higher growth and processing temperatures that have hindered their earlier development.

It was not until advanced growth techniques, including molecular beam epitaxy (MBE) and metal-organic chemical vapor deposition (MOCVD), became available that practical devices based on these materials were realized. The development of light emitting diodes (LEDs) and laser diodes (LDs), operating from the ultra-violet (UV) to the visible, has had a tremendous technological impact. Since there has historically been no native substrate for the growth of the III-N semiconductors, epitaxy has taken place primarily on sapphire (Al_2O_3) or silicon carbide (SiC) substrates. Recently, bulk GaN wafers have become commercially available, but widespred use of these substrates is still in the early stages.

The elements having atomic numbers from 57 to 71 are known as the lanthanide rare earth (RE) elements. While these elements are known as "rare earths", they are actually metals. Their name derives from the difficulty in extracting them from naturally occurring oxide "earths", such as lime and alumina. With increasing atomic number, electrons enter into the underlying 4*f* subshell rather than filling the external 5d shell of these elements. Consequently, the electronic configuration of each lanthanide RE element is often denoted as [Xe] $4f^n$, where [Xe] is the electronic configuration of xenon and n is the number of electrons in the inner 4*f* subshell.

When incorporated into a host material, the RE atom tends to form a trivalent ion (RE^{3+}). In this state, the electronic structure of RE^{3+} ion consists of completely filled outer $5s^2$ and $5p^6$ subshells and a partially filled inner 4*f* subshell. Electron transitions between the 4*f* energy levels give rise to very sharp spectral emissions that range from the UV to the infrared (IR) region depending upon the specific RE element.[2] RE elements are the basis of many optical components, including the solid-state Nd:YAG laser and the erbium doped fiber amplifier.

The magnetic properties of the RE elements have also received a great deal of scientific attention. In general, the magnetic characteristics are due to the spin and orbital motion of the unpaired 4*f* electrons.[3] All of the RE^{3+} ions except the La^{3+} and Lu^{3+}, are paramagnetic, i.e. the electron spins try to align themselves with an applied magnetic field (H_a). The La^{3+} and Lu^{3+} ions are diamagnetic, i.e. the orbiting electrons oppose the H_a field, since La^{3+} has no 4*f* electrons and all of the 4*f* electrons in Lu^{3+} are paired. An important feature is that the RE^{3+} ions from Gd^{3+} to Tm^{3+} become ferromagnetic at very low temperatures, i.e. their magnetic response is non-linear and depends on the history of the applied field. Above a certain temperature, the Néel temperature (T_N), these ions become paramagnetic. Based on quantum mechanics calculations, Van Vleck developed a theoretical model describing the magnetic susceptibilities for the lanthanide RE^{3+} ions.[4] Results of these calculations indicated that the effective magnetic moment (μ_{eff}) is larger for the heavier RE^{3+} ions, those from Gd^{3+} to Tm^{3+}, than for the lighter ones, from Ce^{3+} to Eu^{3+}. Table I contains the calculated magnetic moments of the RE elements that we have investigated, along with their atomic, covalent, and ionic radii data.[5]

Numerous approaches have been used to incorporate RE elements in III-N semiconductor materials. Early research efforts involved ion RE implantation of thin films, solid-state diffusion, and pulsed laser deposition. Eventually, synthesis methods, based on MBE and MOCVD, were developed for in situ doping of III-N films with a wide variety of RE elements.[6–11] In comparison with earlier techniques, in situ RE doping during epitaxial growth has several important advantages including higher crystallinity of the thin films and a more homogeneous RE depth profile. Furthermore, epitaxial growth allows the RE ions to be incorporated into quantum well structures and isolated quantum dots for device applications.

Initial research into RE-doped III-N (III-N:RE) layers focused on the optical emission, at room temperature (RT), in the visible and IR regions.[12,13] Subsequently, research studies of the magnetic properties of such materials ensued. This research was motivated by efforts to develop a dilute magnetic semiconductor (DMS) through doping of III-V semiconductors with transition metal (TM) atoms. In spite of many experimental efforts RT operation could not be demonstrated. However, theoretical calculations indicated that a wide bandgap material such as GaN or ZnO, doped with Mn could lead to a DMS material at RT.[14] Following initial experimental confirmation, research also began concerning doping III-N layers with RE elements as another DMS material with RT effects. Since then, many experimental and theoretical studies have been reported the RT magnetic behavior of different RE elements incorporated into III-N layers.[15]

*Electrochemical Society Member.
[z]E-mail: jmz2018@nyu.edu

Table I. Summary of atomic, covalent, and ionic radii; and, magnetic moments of the rare earth elements treated in this manuscript. Here *g* is the Landé factor, *J* is the total angular momentum, and μ_B is the Bohr magneton. (after 5).

			Ionic radii (pm) coordination number = 8			Magnetic moment (μ_B) $\mu_{eff} = g\sqrt{J(J+1)}\mu_B$		
	Atomic radii (pm)	Covalent radii (pm)	RE^{2+}	RE^{3+}	RE^{4+}	RE^{2+}	RE^{3+}	RE^{4+}
Er	175.7	189		100			9.58	
Gd	180.1	196		106			7.94	
Eu	204.2	198	125	107		7.94	0 (3.4)	
Nd	182.1	201		112			3.62	
Tm	174.6	190	108	99		4.54	7.56	

The focus of the next section is on reports of the synthesis of RE-doped III-N thin films and measurements at RT of magnetic effects of five RE elements (Er, Gd, Eu, Nd, and Tm) introduced into binary and ternary III-N compounds. These RE elements were selected because of their importance in optical device applications and also because of the wide range of magnetic properties that they cover.

Magnetic Properties of III-N:RE

Erbium.—The trivalent Erbium ion (Er^{3+}) has the electron configuration of [Xe] $4f^{11}$ and intra-$4f$ transitions lead to optical emissions at ~1.54 μm. In addition, Er^{3+} has a relatively small ionic radius, ~100 pm, and a large $\mu_{eff} \sim 9.58\ \mu_B$, see Table I. These properties have made Er an important constituent of optical and magnetic components.

Mackenzie et al. used gas source MBE (GS-MBE) for in situ doping of Er into AlN and GaN epilayers.[6] Er concentration (C_{Er}) was $\sim 3 \times 10^{18}$ cm^{-3}, as measured by secondary ion mass spectrometry (SIMS). High levels of impurity elements, O and C, were also observed in the Er-doped films. Later Bang et al. studied the magnetic properties of Er-doped GaN (GaN:Er) films grown on sapphire (0001) substrates also using GS-MBE.[16] Rutherford backscattering (RBS) measurements indicated that C_{Er} was ~ 3 at.%. Sharp luminescence peaks in the visible (green) and IR spectral regions were observed. Magnetization vs applied H field (M vs H_a) measurements were made using a Super Conducting Quantum Interference Device (SQUID) magnetometer and data indicated mainly paramagnetic ordering of Er ions, with only a small portion being ferromagnetic.

A major advance was made by Ugolini et al. with the synthesis of GaN:Er films by MOCVD.[9] In order to achieve sufficiently high Er doping levels in the epilayers, adaptations were made to the MOCVD system. SIMS analysis indicated C_{Er} levels up to $\sim 2 \times 10^{21}$ cm^{-3} were achieved. Impurity concentrations of C and H were $\sim 5 \times 10^{18}$ cm^{-3}, and $<10^{17}$ cm^{-3} for O. X-ray diffraction (XRD) rocking curve measurements indicated that the FWHM was nearly the same as that for undoped GaN films. Magnetic properties of these GaN:Er films were measured by Zavada et al.[17] Results of M vs H_a measurements, using Alternating Gradient Magnetometry (AGM), for a sample having $C_{Er} \sim 10^{21}$ cm^{-3} are shown in Figure 1a. Hysteretic behavior and saturation magnetization (Ms) were observed at 10K and 300K. SQUID magnetization vs temperature (M vs T) measurements, shown in Figure 1b, indicated that the temperature at which the field-cooled (FC) and zero-field-cooled (ZFC) curves coincide was >300K. Measurements that were performed on an undoped GaN sample did not show any magnetic hysteresis.

Nepal et al. studied the influence of light on the magnetic properties of GaN:Er epilayers grown by MOCVD.[18] AGM measurements of GaN:Er samples were made at RT with, and without illumination, from a commercially available LED operating at 371 nm. Diamagnetic properties of the substrate and holder were subtracted out and the data was normalized to sample volume. In Figure 2a, hysteretic data taken at RT, with and without illumination, are presented for a GaN:Er sample with $C_{Er} \sim 2 \times 10^{20}$ cm^{-3}. While the coercivity (H_c) remained constant, there was an increase of ~ 0.8 μemu in M_S when the sample was illuminated. The largest increase in Ms was observed for the sample with the lowest Er concentration. When the LED was turned off, M_S for the sample returned to its original level. Magnetoresistance Hall measurements were performed on the GaN:Er samples and compared to a GaN:Si film also grown by MOCVD. As shown in Figure 2b, the resistance of the GaN:Si film had a linear dependence on H_a, indicating the ordinary Hall effect (OHE). However, the resistance of the GaN:Er sample had a nonlinear dependence, characteristic of the anomalous Hall effect (AHE). The additional voltage component was due to the magnetization of the GaN:Er sample providing evidence of RT ferromagnetic behavior.

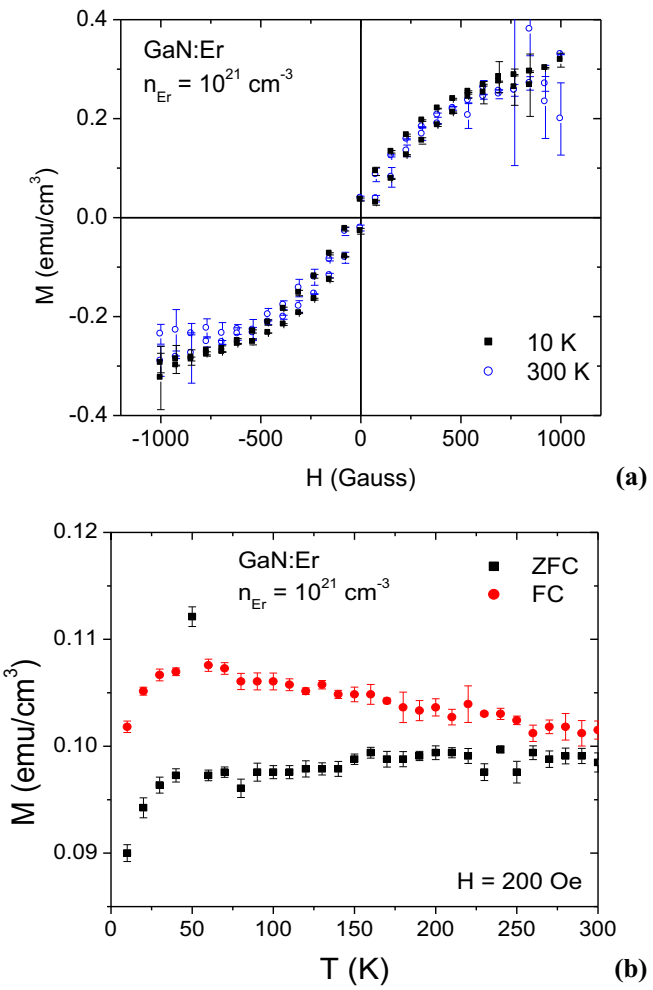

Figure 1. Magnetization data for a GaN:Er sample having $C_{Er} \sim 10^{21}$ cm^{-3}: (a) AGM measurements showing hysteretic behavior at 10K and 300 K; (b) FC and ZFC curves measured with H_a field of 200 Oe.[17]

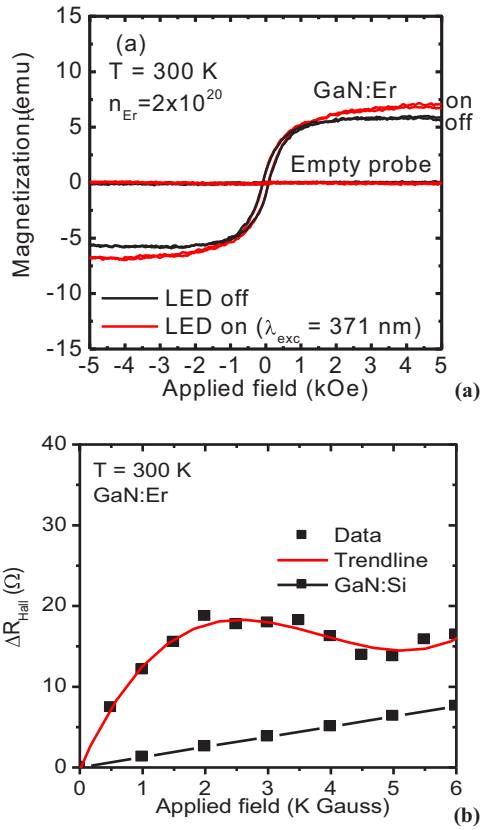

Figure 2. (a) AGM measurements made at RT showing hysteretic behavior under LED on/off illumination for a GaN:Er sample with $C_{Er} \sim 2 \times 10^{20}$ cm^{-3}.[18] (b) Magneto-resistance ΔR_{Hall} data measured at 300K for a GaN:Er epilayer indicating Anomalous Hall behavior.[19]

Er-doping of InGaN was also pursued since this ternary compound was critical in the development of the blue laser.[1] Ugolini succeeded in growing $In_xGa_{1-x}N$:Er films on (0001) sapphire substrates using MOCVD.[20] Growth temperature (T_G) was 760°C and the epilayers had $C_{Er} \sim 1.3 \times 10^{19}$ cm^{-3}. The In content (x) range was from 0.11 to 0.18. Magnetic characterization of these films was made using AGM.[21] In Figure 3, the results of M vs H_a measurements made at RT for InGaN:Er epilayers having different In content are shown. Hysteresis

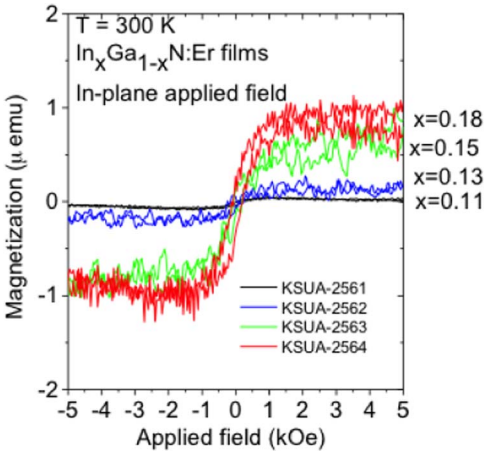

Figure 3. M vs H_a measurements made at RT for $In_xGa_{1-x}N$:Er epilayers grown on sapphire substrates and having different In content x.[21]

curves and magnetic saturation were observed for all samples and Ms was found to increase linearly with In content.

Gadolinium.—The trivalent Gadolinium ion (Gd^{3+}) has an electron configuration of [Xe] $4f^7$ and an ionic radius ~ 106 pm. Its $4f$ electrons produce a relatively large $\mu_{eff} \sim 7.94\ \mu_B$, see Table I. This RE element has found widespread use as a green phosphor.

Teraguchi et al. were the first to study the magnetic properties of Gd-doped GaN (GaN:Gd).[22] The semiconductor layers were grown using plasma-assisted MBE (PA-MBE) on SiC substrates. Elemental Ga and Gd sources were used together with plasma-enhanced N_2. The Gd concentration (C_{Gd}) was ~ 6 at. % based on X-ray photoemission spectroscopy (XPS). M vs H_a measurements were taken using SQUID at temperatures from 7 K to 300 K for the GaN:Gd sample and hysteresis curves were observed at both temperatures indicating ferromagnetic behavior. The saturation field was about 2 Tesla and the H_c was ~ 70 Oe at 300 K. The Curie temperature (T_c) was estimated to be higher than 400 K.

In 2005, Dhar et al. reported a "colossal" effective magnetic moment for GaN:Gd epilayers grown by reactive MBE (R-MBE) on 6H-SiC (0001) substrates.[23] The C_{Gd} ranged from 7×10^{15} cm^{-3} to 2×10^{19} cm^{-3} as measured by SIMS. M vs H_a measurements of these layers indicated that the average value of the μ_{eff} per Gd atom was as high as 4000 μ_B. Since the GaN:Gd samples were electrically highly resistive, long-range coupling via a version of carrier-mediated RKKY (Ruderman-Kittel-Kasuya-Yosida) mechanism did not seem to apply.

In a further report, Dhar et al. stated that the GaN:Gd layers constituted a very dilute, ferromagnetic semiconductor with a $T_c >$ RT.[24] SIMS measurements for different GaN:Gd layers showed that C_{Gd} was nearly uniform throughout the layer at levels from ~10^{17} cm^{-3} to 10^{19} cm^{-3}. Dhar et al. also investigated the magnetic properties of Gd-doped GaN layers produced using a focused ion beam.[25] M vs H_a SQUID measurements, made 2K and 300K, indicated ferromagnetic behavior with $T_c >$ RT. Furthermore, the μ_{eff} per Gd atom in these samples was an order of magnitude larger than values observed in epitaxially grown layers with similar Gd concentrations. The authors concluded that defects due to ion implantation were involved with producing this higher magnetic moment.

Zhou et al. reported GaN:Gd layers, grown by PA-MBE at temperatures below 300°C on sapphire substrates, with C_{Gd} levels as high as 12.5%.[26] The samples exhibited hysteresis behavior at RT with Ms values increasing with higher C_{Gd} levels. The large Ms values were attributed to defects, introduced during growth that enhanced magnetic properties. To investigate this effect, Si was introduced in situ during growth in order to directly increase carrier density. While hysteresis and Ms was observed for all samples, Ms for the Si-doped samples was ~ 7x higher than those non-doped with Si.

Magnetic properties of GaN:Gd layers grown by PA-MBE were examined by Hite et al.[27] Crystal quality and C_{Gd} levels were varied by control of the Gd cell temperature (T_{Gd}) during growth. The C_{Gd} level was estimated to be less than 10^{17} atom/cm^3. Magnetic SQUID measurements showed hysteretic behavior at RT, with the Ms dependent on both C_{Gd} and the crystalline quality of the layer. Samples grown at $T_{Gd} = 1050$°C had the highest crystal quality. In Figure 4a data from M vs H_a measurements, made at 10K and 300K, are shown indicating ferromagnetic behavior with T_c above RT. Data from M vs T measurements are shown in Figure 4b. The lack of closure of the FC and ZFC curves at 300 K also indicated $T_c >$ RT.

Hite et al. also investigated co-doping of GaN:Gd layers with Si to determine whether additional shallow donors in the layer would affect the ferromagnetic behavior.[27,28] The films were grown using solid Ga, Gd, and Si sources. The Si cell temperature (T_{Si}) was varied between 1000 and 1200°C while maintaining $T_{Gd} = 1050$°C. Carrier concentrations reaching 1.45×10^{18} cm^{-3} were achieved and the co-doped GaN:Gd,Si films were n-type conducting with resistivity ~0.04 Ω·cm. In Figure 5, magnetic data from M vs H_a measurements, and from M vs T measurements, are shown. Hysteretic behavior at RT was observed for the co-doped GaN:Gd,Si layers, with higher Ms values than that the non-Si-doped films.

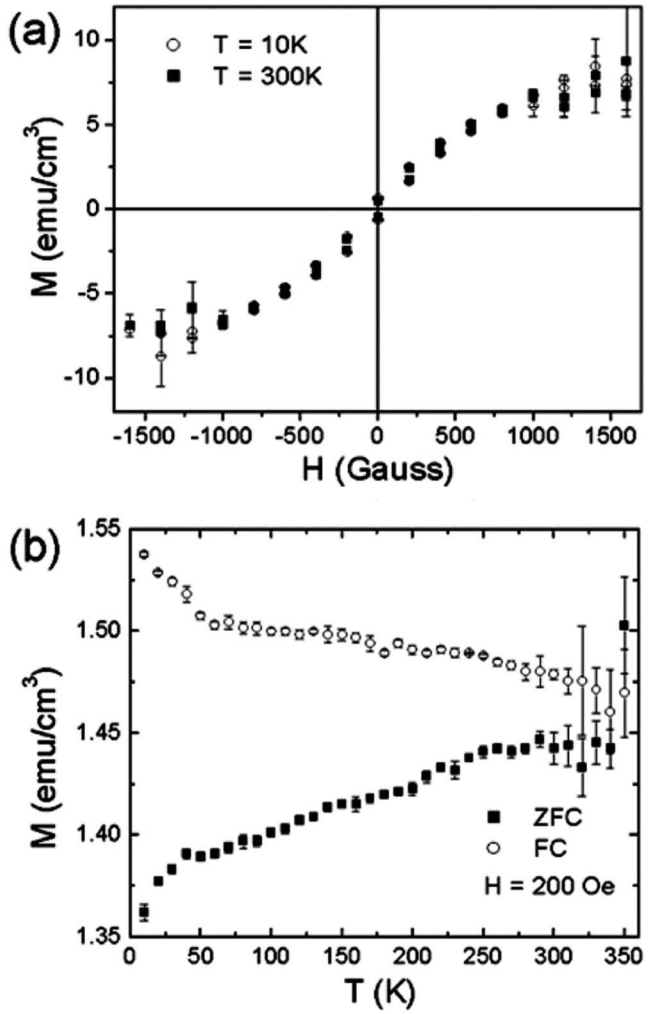

Figure 4. Magnetic measurements for a GaN:Gd film grown by PA-MBE at $T_{Gd} = 1050°C$: (a) M vs H_a data made at 10K and 300K; (b) M vs T data, with $H_a \sim 200$ Oe, showing closure of FC and ZFC curves at ~ 300 K.[27]

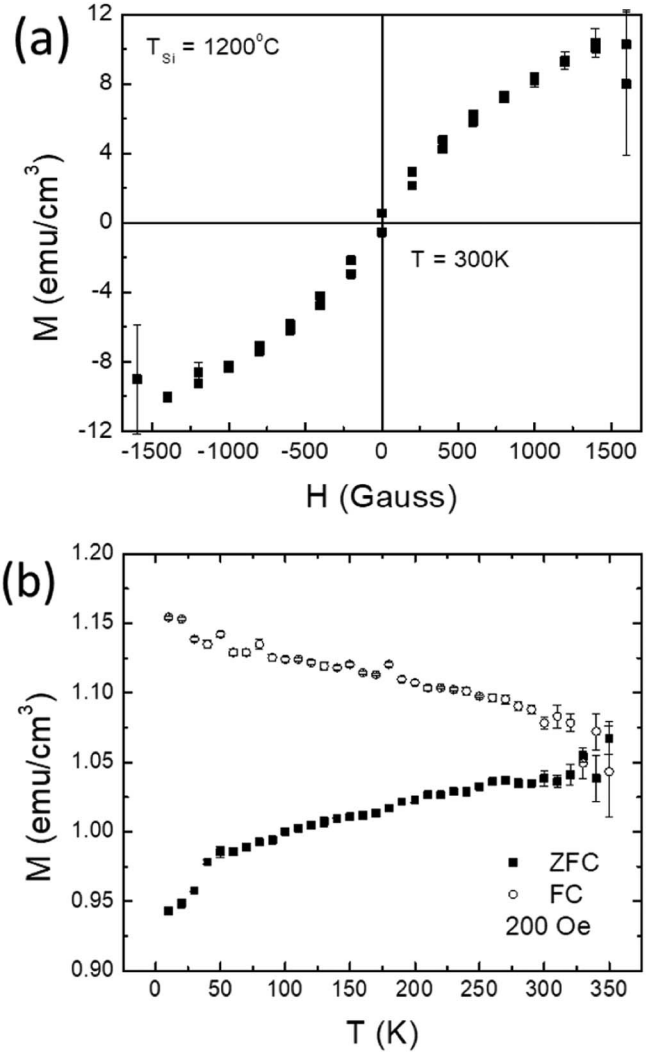

Figure 5. (a) M vs H_a data at 300 K for a co-doped GaN:Gd,Si film grown with Si cell $T_{Si} = 1200°C$; (b) M vs T data, with $H_a \sim 200$ Oe, showing closure of FC and ZFC curves at ~ 300 K.[28]

Gupta et al. succeeded in growing GaN:Gd layers by MOCVD and investigated the relationship of the chemical, magnetic, and electrical properties of these films.[11] These layers were found to be ferromagnetic and electrically conducting at RT. The effect of co-doping was studied and GaN:Gd films were grown with either Si or with Mg co-dopants. Data from M vs H_a measurements, taken at RT, indicated that co-doping the films, with either Si or Mg, resulted in an increase in the Ms as compared with the non-co-doped layers.

The effects of proton irradiation on the magnetic properties of GaN:Gd layers were investigated by Hite et al.[29] The layers were grown by PA-MBE on GaN substrates. The C_{Gd} level was on the order of 10^{16} atom/cm^3. The films were irradiated with 10 and 40 MeV protons at a fluence of 5×10^9 cm^{-2}. The projected range of the protons was > 40 μm, which was much greater than the thickness of the epitaxial films, ~ 1500 Å. After irradiation, the optical and magnetic properties of the films were measured. The PL band edge emission, following irradiation at 10 MeV, was reduced by more than 50%. SQUID measurements also showed a decrease in magnetic properties with a reduction up to 83% in Ms. However, following a 30 minute anneal at 500°C under N plasma, the irradiated films showed a complete recovery of magnetic behavior. In Figure 6, M vs T data, taken at $H_a = 200$ Oe, are shown for a GaN:Gd layer before proton irradiation at 10 MeV, and after annealing. The authors concluded that irradiation damage, in the form of deep traps, produced the changes in the optical and magnetic properties and that these effects were reversible.

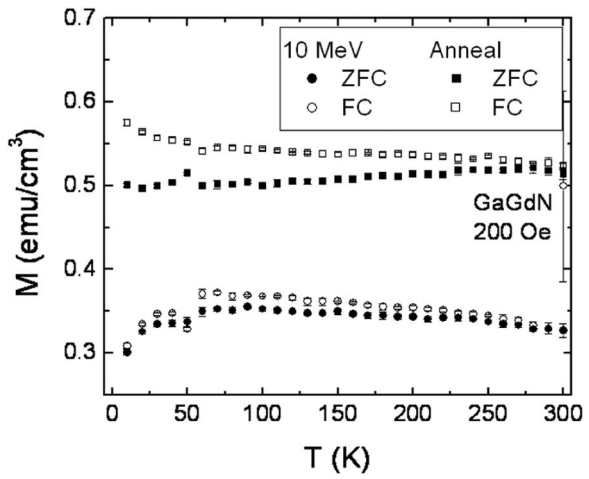

Figure 6. M vs T data for a GaN:Gd sample exposed to 10 MeV proton irradiation, before and after annealing. Irradiated data points are shown as circles, and those from the annealed sample are denoted as squares. Error bars are shown on all points.[29]

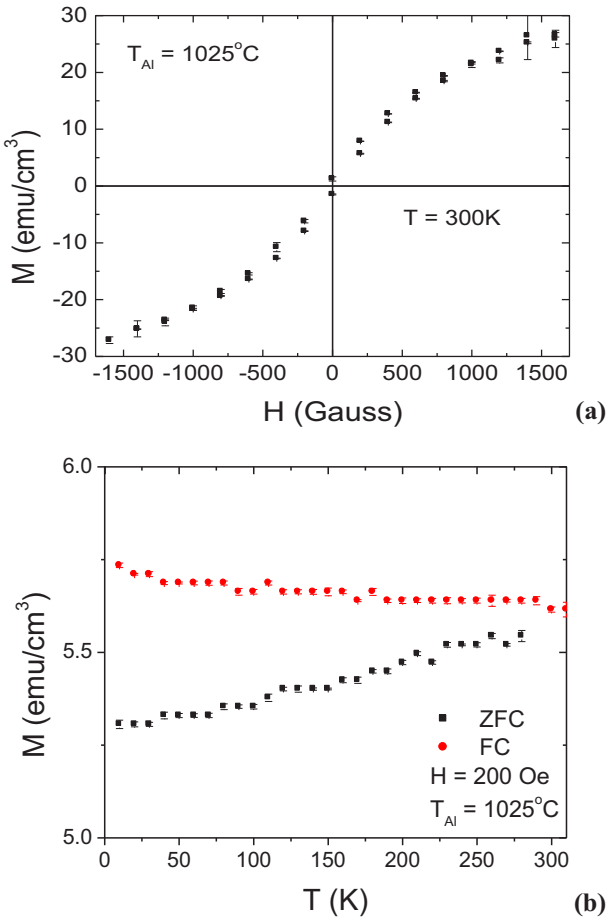

Figure 7. (a) Magnetization vs H_a field curve shown for T_{Al} = 1025°C (26% Al). These measurements were taken at 300K. The 10K traces overlap those shown at 300K. (b) Magnetization vs T curves show both ZFC and FC traces at an applied field of 200 Oe.[35]

Doping of ternary InGaN compounds with Gd has also been achieved. Tawil et al. grew InGaN:Gd layers using PA-MBE on GaN (0001) templates.[33,34] Growth at 400°C produced an In content up to 28% and 35% and C_{Gd} levels ~1 at. %. Data from M vs H_a measurements made at RT exhibited clear hysteretic behavior with M_S levels increasing with higher C_{Gd} levels. Co-doping the InGaN:Gd layers with Si was also investigated and an increase in magnetization was observed with higher Si cell temperatures. Electrical properties were measured and indicated a correlation between the film conductivity and Ms. The authors concluded that the results provided evidence of carrier-mediated ferromagnetism.

Doping of AlGaN with Gd has also been accomplished using PA-MBE on GaN (0001) templates by Hite.[35] These samples were also found to be ferromagnetic. In samples with Al content ranging from 40–62%, the M_S increased with Al content, but at overall levels that were lower than similarly grown binary doped samples. However, for $Al_{0.26}Ga_{0.74}N$:Gd, M_S was much higher than the binary values. In Figures 7a and 7b show the M vs. H and M vs. T measurements, supporting room temperature ferromagnetic behavior. Correspondingly, at this composition, the films showed the highest conductivity and the highest crystal quality. Annealing under N_2 plasma at 700C for 30 minutes showed a drastic degradation of the magnetization.

Additionally, multiquantum wells with Gd-doped binaries and ternaries were investigated by Hite.[35] These included structures of GaN:Gd/AlN, GaN:Gd,Si/AlN, and AlGaN:Gd/GaN. In all the cases, thinning the Gd-doped layers reduced the magnetic saturation of the layers relative to that of bulk Gd-doped films of equivalent thicknesses.

Major disagreements remain concerning the magnetic properties of GaN:Gd samples with very low concentrations of Gd. Wang et al. characterized the magnetization of GaN thin films implanted with Gd ions at very low doses.[30] They found that the μ_{eff} per Gd ion was ~ 1800 μ_B, which is comparable to the values reported by Dhar et al. However, they observed that the ferromagnetic response was metastable and that after ~ 50 days values for μ_{eff} returned to those of the un-implanted samples. Their conclusion was that the magnetic effects found in Gd-implanted GaN specimens were defect-related.

Bedoya-Pinto et al. investigated GaN:Gd samples grown by MBE with low Gd concentrations. The samples were grown on highly insulating SiC substrates to avoid parallel conduction through the substrate or in the interface layer. Hysteretic behavior at RT was observed with values for μ_{eff} per Gd ion comparable to those reported by Dhar et al. However, in some samples there was a decrease in Ms over extended time periods and an overall poor reproducibility of magnetic results. The authors reported that variable range hopping in electrical transport could have influenced the ferromagnetism.[31,32]

Europium.—The trivalent Europium ion (Eu^{3+}) has the electron configuration of [Xe] $4f^6$ and a relatively large ionic radius of ~107 pm, making it difficult for doping III-nitride materials, see Table I. In addition, the ground state of Eu^{3+} ($^7F_0$) nominally indicates absence of a magnetic moment. However, various studies have reported magnetic properties of Eu-doped GaN (GaN:Eu) layers. Due to interactions of Eu ions with defects in the host GaN material, Eu^{3+} can possess remnant magnetization with a finite magnetic moment, with μ_{eff} per Eu atom ~ 3.4 μ_B.

Using solid source MBE (SS-MBE), Heikenfeld et al. demonstrated in situ doping GaN films with Eu.[36] The films were grown on Si substrates and SIMS analysis indicated low levels of O and other impurities. The films exhibited strong photoluminescence (PL) emission with a spectrum that was consistent with Eu^{3+} ions occupying Ga sites. Electroluminescence (EL), based on electron impact excitation, yielded bright red emission from the GaN:Eu films.

Magnetic properties of GaN:Eu layers were first studied by Hashimoto et al.[37] The films were grown by grown by GS-MBE using NH_3 on (0001) sapphire substrates. Results of M vs H_a measurements showed magnetic saturation and slight hysteresis indicating the presence of both paramagnetic and ferromagnetic phases. To explain the experimental results, the authors proposed a theoretical model based on the presence of Eu^{2+} ions and Eu^{3+} ions interacting through a type of RKKY interaction.

Optical and magnetic properties of GaN:Eu films, grown on *c-plane* sapphire substrates by SS-MBE, were measured by Hite et al.[38] Results of M vs H_a SQUID measurements were made at RT. Hysteresis and magnetic saturation were observed in as shown in Figure 8a. Data from M vs T measurements are shown in Figure 8b. The lack of closure of the FC and ZFC curves at 300 K indicated T_c ~ RT. An inverse correlation was found between the PL emission intensity from Eu^{3+} ions and Ms levels in these samples.

Electric and magnetic properties of Eu and Si co-doped GaN films (GaN:Eu,Si), grown by SS-MBE, were investigated by Wang et al.[39] The Si concentration was found to depend monotonically on the Si cell temperature (T_{Si}). Incorporation of Si changed the GaN:Eu films from highly resistive to n-type conductive. Magnetic properties of the GaN:Eu,Si films were measured using AGM. While all samples exhibited hysteresis behavior at RT, there was a marked dependence on the Si co-doping. In Figure 9a data from M vs H_a measurements at RT are shown for the samples grown with T_{Si} = 1050°C and T_{Si} = 1100°C. At low-to-moderate Si levels, an increase up to approximately nine times in Ms was realized. The Ms reached a maximum with growth at T_{Si} ~1100°C and then decreased for higher temperatures.

Magneto-resistance Hall measurements were performed on the GaN:Eu,Si film, grown with T_{Si} ~1150°C, and on a GaN:Si film grown by MOCVD. As shown in Figure 9b the resistance of the GaN:Si film had a linear dependence on H_a (OHE) whereas the GaN:Eu,Si film had a nonlinear dependence (AHE). The nonlinear behavior provided

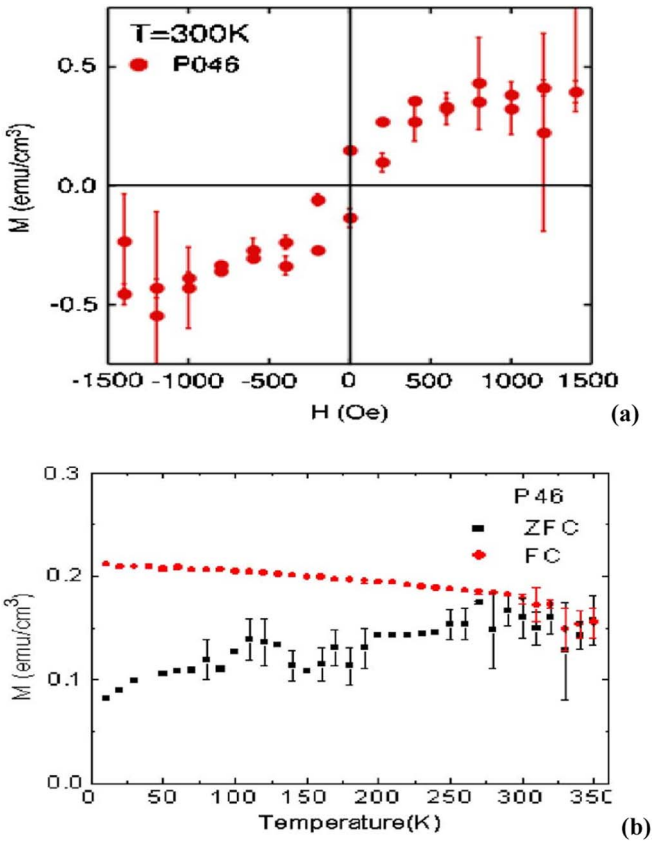

Figure 8. Magnetic measurements for a GaN:Eu sample grown by SS-MBE: (a) M vs H_a data taken at RT showing hysteretic behavior; (b) M vs T data, with $H_a \sim 200$ Oe, with closure of FC and ZFC curves at ~ 300 K.[38]

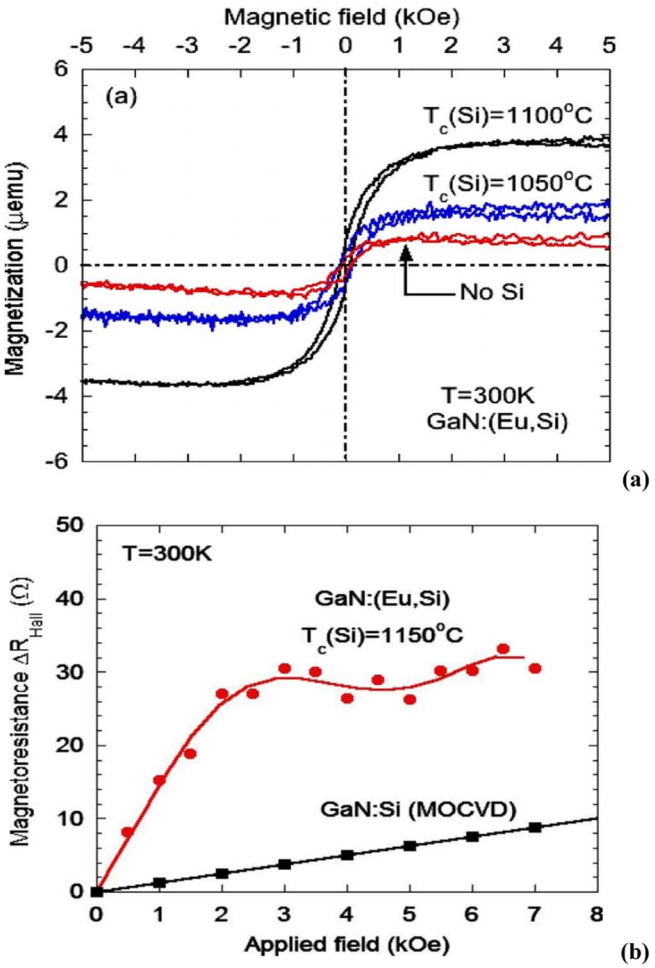

Figure 9. (a) M vs H_a hysteresis curves measured at 300 K for the co-doped GaN:Eu,Si sample. Data for a non-Si doped GaN:Eu film are also shown; (b) Magneto-resistance ΔR_{Hall} data measured at RT for the co-doped sample grown with $T_{Si} \sim 1150$°C. Data for a GaN:Si film grown by MOCVD are also shown.[39]

further evidence of ferromagnetic behavior for the co-doped GaN:(Eu,Si) samples.

Neodymium.—The trivalent Neodymium ion (Nd^{3+}) has the electron configuration [Xe] $4f^3$. Intra-4*f* transitions in Nd^{3+} give rise to IR emissions centered at ~1.04 μm. These transitions form the basis of a number of important solid state lasers, in particular Nd:YAG.[40] The Nd^{3+} ion has an ionic radius of ~ 112 pm, and its 4*f* electrons lead to μ_{eff} per Nd atom $\sim 3.62\ \mu_B$, see Table I. While the optical properties of Nd doped materials have been widely studied, only a few reports deal with magnetic properties of Nd in semiconductors.

Two methods have been used use to introduce Nd ions into GaN films: solid-state diffusion, and MBE. Luen et al. investigated the thermal diffusion of several different RE elements into GaN thin films including Nd.[41,42] GaN layers, including undoped GaN, p-GaN:Mg, and n-GaN:Si, were grown by MOCVD on sapphire substrates to serve as templates for the Nd diffusion experiments. Optimization of the diffusion conditions led to successful incorporation of Nd into the GaN films as evidenced by SIMS. M vs H_a measurements at RT were made using AGM. The H_a field strength varied from −5kOe to +5kOe for both in-plane and out-of-plane orientations. Hysteretic behavior was observed for all samples, see Figure 10. While the measured H_c was ~100 Oe for all samples, the highest Ms was found for Nd diffused into the p-GaN:Mg template.

Magneto-resistance measurements were performed at RT on a Nd-diffused GaN:Si sample and on an as-grown GaN:Si template. The Nd-diffused GaN:Si sample had a nonlinear relationship, indicating an anomalous Hall effect (AHE), see Figure 11. In addition, the as-grown GaN:Si template did not show magnetic hysteresis in AGM measurements.

Readinger et al. reported in situ Nd doping of GaN epilayers grown on *c-plane* sapphire substrates using PA-MBE.[43,44] Based on RBS and SIMS measurements, the GaN:Nd films had Nd concentrations (C_{Nd}) ranging from 0.004% to 6.0%. PL measurements were made at RT using a pump laser at 266 nm and IR spectra with the characteristic peaks from the 4*f* transitions for Nd^{3+} ions were observed. Bandedge luminescence was also measured in the region of ~ 360 nm for each of the GaN:Nd samples. As the sample C_{Nd} increased, a significant decrease in the PL bandedge emission intensity (I_{emi}) was observed. For samples with $C_{Nd} > 1.0$ at. % nearly all of the bandedge luminescence was suppressed.

Magnetic properties of the GaN:Nd samples were measured at RT using AGM for both in-plane and out-of-plane orientations. The out-of-plane orientation yielded only weak magnetic signals. Typical magnetization curves for in-plane orientation, with hysteretic behavior, are shown in Figure 12a. It can be seen that the Ms was largest for the GaN:Nd sample with $C_{Nd} \sim 6.0\%$ Nd. However, when both the Ms and the I_{emi} are normalized to Nd atom density, then a strong correlation appears, see Figure 12b. Two main features are noticeable. First, the shape of the curve for the bandedge I_{emi} and that for the μ_{eff} per Nd atom is nearly the same; they can almost be superimposed. Second, for the lowest C_{Nd}, μ_{eff} per Nd atom is very high, $\sim 55\ \mu_B$. While this value is not as high as estimates reported for Gd, it is much higher than the theoretical value. Furthermore, as the C_{Nd} was increased, the μ_{eff} per Nd atom decreased to values consistent with predicted value of $\sim 3.62\ \mu_B$ per Nd atom.

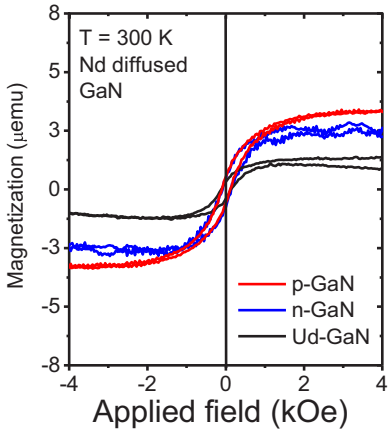

Figure 10. M vs H_a hysteresis curves measured at RT for Nd diffused into: p-GaN:Mg; n-GaN:Si; and, undoped Ud-GaN. Diffusion into a doped substrate increased Ms.[41]

Thulium.—The trivalent Thulium ion (Tm^{3+}) has the electron configuration of [Xe] $4f^{12}$. It has a small ionic radius of ~ 99 pm, and a relatively large $\mu_{eff} \sim 7.56\ \mu_B$, see Table I. Intra-4*f* transitions in Tm^{3+} give rise to IR emissions centered at ~ 2.08 μm that transitions form the basis of an important class of tunable lasers.[40]

Steckl et al. were able to grow Tm-doped GaN films on *p-type* Si (111) substrates using solid-source MBE with a rf-plasma source to supply atomic N. Light emitting devices were prepared and strong blue EL emission, centered at ~ 477 nm, was observed.[45] In order to enhance the EL of these devices, Lee and Steckl grew a set of AlGaN:Tm thin films also on *p-type* Si (111) substrates. The Al content (x) covered the entire compositional range of $0 \leqslant x \leqslant 1$. The Tm concentration ($C_{Tm}$) was ~ 0.2–0.5 at. % and all films were capped with an un-doped $Al_xGa_{1-x}N$ layer. The intensity of blue EL emission increased monotonically with Al composition, from $x = 0$ for to $x \sim 0.8$.[46] Using a laser source at 250 nm, Hömmerich et al. measured the PL spectra of the same set of samples and found a similar increase in the blue emission intensity as a function of Al composition.[47] The emission intensity reached a maximum for the alloy with $x = 0.62$. Since the bandgap of the $Al_xGa_{1-x}N$ alloys increased with higher Al content, they were able to observe additional emission lines in the UV region.

Magnetization of the AlGaN:Tm samples was measured at RT using AGM with both in-plane and out-of-plane field orientations.[48] The easy axis of magnetization for these alloys was along the in-plane direction. Results of the AGM measurements showed hysteretic behavior at RT for each sample except for $x = 0$, see Figure 13a. The hysteresis curve for the GaN:Tm sample was nearly flat, indicating paramagnetic behavior. In addition, the measured magnetization was strongly dependent upon the Al content and reached a maximum for $x = 0.62$ alloy, Figure 13b.

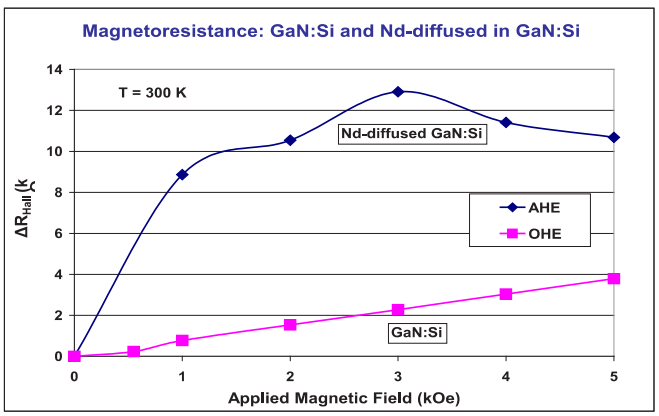

Figure 11. Magneto-resistance data, ΔR_{Hall}, measured at RT, for the Nd-diffused GaN:Si sample and for the as-grown GaN:Si template. The solid lines serve as a guide for the eyes.[42]

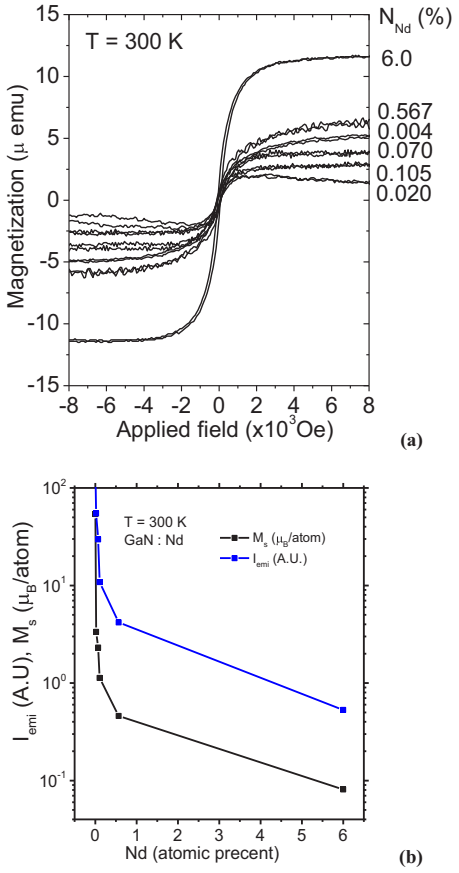

Figure 12. (a) M vs H curves measured at RT with in-plane orientation for GaN:Nd samples having different C_{Nd} values; (b) Comparison of the normalized Ms and the bandedge emission intensity I_{emi} measured at RT for the GaN:Nd samples.[44]

Summary and Discussion

While several methods have been developed for doping RE elements into III-N semiconductors, MBE and MOCVD appear to be the most successful. Every lanthanide RE element has been successfully introduced into a III-N semiconductor host. While thin films of GaN have been the primary host material, other III-N hosts have included AlN, InGaN, and AlGaN alloys. In spite of the large mismatch between the RE ionic radius and that of either Ga or Al or In, high quality layers of III-N:RE have been produced.

Initial work centered on the optical properties of RE-doped III-N materials. Many issues concerning synthesis and processing of III-N:RE layers have been studied and resolved. The optical studies focused on developing new materials for efficient light emission at different wavelengths for full-color displays. Results of these studies have proved useful for the subsequent magnetic investigations.

While most RE-doped MBE and MOCVD growth has taken place either on sapphire or SiC substrates, there have been a few reports of growth on Si substrates. The use of different substrates for III-N:RE synthesis affects both the resulting thin film crystal quality as well as the optical properties. Magnetic properties are also influenced by the stress in the GaN:Er film induced by lattice mismatch between the epilayer and the substrate.[49] At low rare earth doping levels,

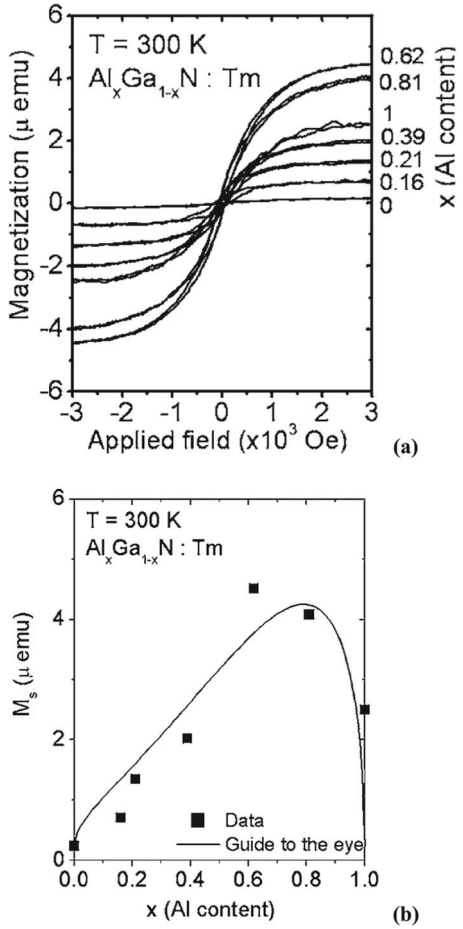

Figure 13. Magnetization data for the Tm-doped $Al_xGa_{1-x}N$ alloys covering the compositional range of $0 \leqslant x \leqslant 1$. (a) M vs H_a curves measured at 300 K with in-plane orientation; (b) Variation of the Ms with Al content (x). The solid line is a guide for the eyes.[48]

~ 1 at. %, XRD measurements have shown that the III-N:RE epilayers have good crystal quality without evidence of second phases.

A wide range of experimental techniques, including M vs H_a, M vs T, and magneto-resistance Hall measurements, have been used to characterize the magnetic properties of the III-N:RE layers. Based on these studies, a number of research groups have reported ferromagnetic properties of such layers. While the observed magnetization has been weak, most investigations have reported hysteresis curves at RT, non-closure of FC/ZFC data in SQUID measurements, and anomalous Hall behavior. These experimental reports, prepared by different groups using different synthesis methods and different substrates, provide strong evidence of III-N:RE layers being ferromagnetic materials.

A number of questions still remain concerning the magnetic properties of III-N:RE materials. In particular, the percentage of active magnetic complexes in such materials and their stability at RT are largely unknown. The role and function of co-doping the III-N host material with both a RE and another element needs to be better understood. Several research groups have reported that co-doping the III-N:RE layer, with either Si or Mg, improves the measured magnetization. It is not clear whether this enhancement is due to higher conductivity in the co-doped layer or to better RE ion incorporation in the III-N lattice producing a higher percentage of active magnetic complexes.[50]

Of all the III-N:RE semiconductors that have been investigated, GaN:Gd has received the most attention in both experimental and theoretical studies. This has been due to the reports that μ_{eff} per Gd atom could take on "colossal" values at very low concentrations.[23–25] While these reports involved very thorough experimental studies, subsequent results on GaN:Gd, from other research groups, have called into question such large values of μ_{eff}. Defects and impurities introduced during synthesis or processing may be responsible for reports of extreme values of the μ_{eff} per Gd ion.[51] Concentration levels for impurities, including C, O, and H, have seldomly been reported.

As discussed above, there is controversy concerning the magnetic properties of RE ions in the III-V nitride semiconductor host materials. The same is true with TM ions doped into these semiconductors.[52] These reports have claimed that the ferromagnetic behavior of GaN:TM thin films is due to nanophases in the GaN host material that may also be responsible for some of the GaN:RE behavior.[53,54] While there are similarities between these two material systems, the behavior of RE ions in III-V semiconductors is very different than that of TM ions. Most importantly, the RE ions in GaN tend to form a 3+ charge state and reside on the Ga crystal sub-lattice. The 4*f* transitions of the RE^{3+} ions give rise to a set of very characteristic optical emissions. In the experiments described above, samples were examined using PL and those measurements confirmed the presence of RE^{3+} ions in the GaN host. In contrast, the charge state of TM ions in III-V semiconductors can assume several different values. For GaAs, TM ions usually form a 2+ valency leading to p-type conductivity. However, in GaN, the charge state situation of TM ions is less well understood. Consequently, generalizations concerning these two material systems must be made cautiously.

In our RE-doping experiments, optical, magnetic, and electrical measurements have been performed on various III-N samples, including un-intentionally doped films and those co-doped with either Si or Mg ions. None of undoped samples displayed either 4*f* optical emissions, or magnetic behavior, or the anomalous Hall effect. Co-doping GaN:RE films with Si, or Mg did enhance the magnetic behavior, as was also found in GaN:TM samples. Furthermore, several of our experiments indicated that the magnetic properties of the GaN:RE films can be altered by either the intentional introduction of defects or by LED illumination. These magnetic changes were reversable, as shown in Figures 2a and 6. It is difficult to reconcile such experimental results with a conceptual model for magnetization based solely on the presence of nanophases. Additionally, nanophases or clustering has not been experimentally observed in GaN:RE films; however, the structural characterization, with TEM or atom probe tomography, of these films has not been as widely investigated as with GaN:TM films.

Another issue that has not received sufficient attention is the control of magnetic behavior of III-N:RE materials with an applied electrical field. Nepal et al. fabricated GaN:Mn i-p-n device structures that demonstrated functional control of magnetic behavior at RT using an applied voltage to the GaN p-n junction.[55] No such electrical control of magnetic behavior for a device based on III-N:RE materials has been reported as yet. Nevertheless, doping of wide bandgap semiconductor materials with RE ions is a promising research area with a large potential technological impact for photonic and magnetic device applications.

Acknowledgments

This research was supported in part by the U.S. Army Research Office and the National Science Foundation. Work at the U.S. Naval Research Laboratory is supported by the Office of Naval Research. The authors wish to acknowledge the many people who participated these investigations, in particular: S. J. Pearton, C. R. Abernathy at University of Florida; A.J. Steckl at University of Cincinnati; H.X. Jiang, J.Y. Lin at Texas Tech University; N. El-Masry at North Carolina State, and N. Nepal now at the Naval Research Laboratory.

ORCID

J. K. Hite https://orcid.org/0000-0002-4090-0826
J. M. Zavada https://orcid.org/0000-0001-6219-6748

References

1. S. Nakamura, S. J. Pearton, and G. Fasol, *The Blue Laser Diode: The Complete Story*, 2nd edition, Springer (2000).
2. S. Hufner, *Optical Spectra of Transparent Rare Earth Compounds*, Academic, New York (1978).
3. A. Aharoni, *Introduction to the Theory of Ferromagnetism*, 2nd edition, Oxford Science Publications (2000).
4. J. H. Van Vleck, "*Theory of Electric and Magnetic Susceptibilities"*, Chap. XII, Oxford (1932).
5. For a list of the effective magnetic moments of the RE^{3+} ions, see D. R. Lide, *CRC Handbook of Physics and Chemistry* (2004).
6. J. D. MacKenzie, C. R. Abernathy, S. J. Pearton, U. Hömmerich, X. Wu, R. N. Schwartz, R. G. Wilson, and J. M. Zavada, *Appl. Phys. Lett.*, **69**, 2083 (1996).
7. A. J. Steckl and R. Birkhahn, *Appl. Phys. Lett.*, **73**, 1700 (1998).
8. K. Hara, N. Ohtake, and K. Ishii, *Phys. Status Solidi (b)*, **216**, 625 (1999).
9. C. Ugolini, N. Nepal, J. Y. Lin, H. X. Jiang, and J. M. Zavada, *Appl. Phys. Lett.*, **89**, 151903 (2006).
10. A. Nishikawa, N. Furukawa, T. Kawasaki, Y. Terai, and Y. Fujiwara, *Appl. Phys. Lett.*, **97**, 051113 (2010).
11. S. Gupta, T. Zaidi, A. Melton, E. Malguth, H. Yu, Z. Liu, X. Liu, J. Schwartz, and I. T. Ferguson, *J. Appl. Phys.*, **110**, 083920 (2011).
12. *Photonic Applications of Rare-Earth-Doped Materials*, A. J. Steckl and J. M. Zavada, Guest Editors, *Mater. Res. Soc. Bull.*, **24**(9), 16 (1999).
13. *Rare Earth Doped III-Nitrides for Optoelectronic and Spintronic*, *Applications*, K. O'Donnell and V. Dierolf, Editors, Springer (2010).
14. T. Dietl, H. Ohno, F. Matsukura, and J. Cibert, *Science*, **287**, 1019 (2010).
15. *Rare Earth and Transition Metal Doping of Semiconductor Materials*, *Synthesis*, *Magnetic Properties and Room Temperature Spintronics*, V. Dierolf, I. T. Ferguson, and J. M. Zavada, Editors, Woodhead Publishing, Elsevier (2016).
16. H. Bang, J. Sawahata, G. Piao, M. Tsunemi, H. Yanagihara, E. Kita, and K. Akimoto, *Phys. Status Solidi (c)*, **7**, 2874 (2003).
17. J. M. Zavada, N. Nepal, C. Ugolini, J. Y. Lin, H. X. Jiang, R. Davies, J. K. Hite, C. R. Abernathy, S. J. Pearton, E. E. Brown, and U. Hömmerich, *Appl. Phys. Lett.*, **91**, 054106 (2007).
18. N. Nepal, J. M. Zavada, R. Dahal, C. Ugolini, A. Sedhain, J. Y. Lin, and H. X. Jiang, *Appl. Phys. Lett.*, **95**, 022510 (2009).
19. N. Nepal, C. R. Eddy, J. M. Zavada, S. M. Bedair, N. A. El-Masry, A. J. Steckl, J. Y. Lin, and H. X. Jiang, Presentation, Mater. Res. Soc. Fall Meeting (2010).
20. C. Ugolini, *"Optical and Structural Properties of Er-doped GaN/InGaN Materials and Devices Synthesized by Metal Organic Chemical Vapor Deposition*," *PhD Thesis* Kansas State University (2008).
21. N. Nepal, H. X. Jiang, J. Y. Lin, B. Mitchell, V. Dierolf, and J. M. Zavada, *"MOCVD Growth of Er-doped III-N and Optical-Magnetic Characterization*," *Chapter 7*, *Rare Earth and Transition Metal Doping of Semiconductor Materials*, *Synthesis, Magnetic Properties and Room Temperature Spintronics*, (Editors: V. Dierolf, I. Ferguson, and J. Zavada, Woodhead Publishing (Elsevier, 2016).
22. N. Teraguchi, A. Susuki, Y. Nanishi, Y. K. Zhou, M. Hashimoto, and H. Asahi, *Solid State Commun.*, **122**(12), 651 (2002).
23. S. Dhar, O. Brandt, M. Ramsteiner, V. F. Sapega, and K. H. Ploog, *Phys. Rev. Lett.*, **94**, 037205 (2005).
24. S. Dhar, L. Pérez, O. Brandt, A. Trampert, K. H. Ploog, J. Keller, and B. Beschoten, *Phys. Rev. B*, **72**, 245203 (2005).
25. S. Dhar, T. Kammermeier, A. Ney, L. Pérez, K. H. Ploog, A. Melnikov, and A. D. Wieck, *Appl. Phys. Lett.*, **89**, 062503 (2006).
26. Y. K. Zhou, S. W. Choi, S. Emura, S. Hasegawa, and H. Asahi, *Appl. Phys. Lett.*, **92**(6), 062505 (2008).
27. J. K. Hite, R. M. Frazier, R. Davies, G. T. Thaler, C. R. Abernathy, S. J. Pearton, J. M. Zavada, and R. Gwilliam, *Appl. Phys. Lett.*, **89**, 092119 (2006).
28. J. K. Hite, R. M. Frazier, R. P. Davies, G. T. Thaler, C. R. Abernathy, S. J. Pearton, J. M. Zavada, E. Brown, and U. Hömmerich, *J. Elec. Mater.*, **36**(4), 391 (2007).
29. J. K. Hite, K. K. Allums J., G. T. Thaler, C. R. Abernathy, S. J. Pearton, R. M. Frazier, R. Dwivedi, R. Wilkins, and J. M. Zavada, *New J. of Physics*, **10**, 055005 (2008).
30. X. Wang, C. Timm, X. M. Wang, W. K. Chu, J. Y. Lin, H. X. Jiang, and J. Z. Wu, *J. Supercond. Nov. Magn.*, **24**, 2123 (2011).
31. A. Bedoya-Pinto, J. Malindretos, M. Roever, D. D. Mai, and A. Rizzi, *Phys. Rev. B*, **80**, 195208 (2009).
32. M. Roever, J. Malindretos, A. Bedoya-Pinto, A. Rizzi, C. Rauch, and F. Tuomisto, *Phys. Rev. Lett. B*, **54**, 081201 (2011).
33. S. N. M. Tawil, D. Krishnamurthy, R. Kakimi, S. Emura, S. Hasegawa, and H. Asahi, *J. Cryst. Growth*, **323**, 351 (2011).
34. S. N. M. Tawil, D. Krishnamurthy, R. Kakimi, M. Ishimaru, S. Emura, S. Hasegawa, and H. Asahi, *Phys. Status Solidi C*, **8**, 491 (2011).
35. J. K. Hite, *"Influence of Gadolinium as a Dopant in III-Nitride Dilute Magnetic Semiconductors" PhD Dissertation*, University of Florida (2006).
36. J. Heikenfeld, M. J. Garter, D. S. Lee, R. H. Birkhahn, and A. J. Steckl, *Appl. Phys. Lett.*, **75**, 1189 (1999).
37. M. Hashimoto, A. Yanase, R. Asano, H. Tanaka, H. Bang, K. Akimoto, and H. Asahi, *Jap. J. Appl. Phys.*, **42**, L1112 (2003).
38. J. K. Hite, G. T. Thaler, R. Khanna, C. R. Abernathy, S. J. Pearton, J. H. Park, A. J. Steckl, and J. M. Zavada, *Appl. Phys. Lett.*, **89**, 132119 (2006).
39. R. Wang, A. J. Steckl, N. Nepal, and J. M. Zavada, *J. Appl. Phys.*, **107**, 013901 (2010).
40. R. C. Powell, *Physics of Solid-State Lasers*, (Springer-Verlag, New York, 1998).
41. M. O. Luen, N. Nepal P. Frajtag, J. M. Zavada, E. E. Brown, U. Hommerich, S. M. Bedair, and N. A. El-Masry, *Mater. Res. Soc. Symp. Proc.*, **1183**, FF06-01 (2009).
42. M. O. Luen, *"Spintronics: Towards Room Temperature Ferromagnetic Devices* via *Mn and Rare Earth Doped GaN," PhD Thesis*, *North Carolina State University* (2010).
43. E. D. Readinger, G. D. Metcalfe, H. Shen, and M. Wraback, *Appl. Phys. Lett.*, **92**, 061108 (2008).
44. G. D. Metcalfe, E. D. Readinger, N. Woodward, V. Dierolf, N. Nepal, and J. M. Zavada, *Chap. 9*, *Rare Earth and Transition Metal Doping of Semiconductor Materials*, *Synthesis*, *Magnetic Properties and Room Temperature Spintronics, (*Editors: V Dierolf, I. Ferguson, and J. Zavada, Woodhead Publishing (Elsevier, 2016).
45. A. J. Steckl, M. J. Garter, D. S. Lee, J. Heikenfeld, and R. H. Birkhahn, *Appl. Phys. Lett.*, **75**, 2184 (1999).
46. D. S. Lee and A. J. Steckl, *Appl. Phys. Lett.*, **83**, 2094 (2003).
47. U. Hömmerich, Ei Ei Nyen, D. S. Lee, and J. M. Zavada, *Appl. Phys. Lett.*, **83**(22) 4556 (2003).
48. N. Nepal, S. M. Bedair, N. A. El-Masry, D. S. Lee, A. J. Steckl, and J. M. Zavada, *Appl. Phys. Lett.*, **91**, 222503 (2007).
49. N. T. Woodward, N. Nepal, B. Mitchell, I. W. Feng, J. Li, H. X. Jiang, J. Y. Lin, J. M. Zavada, and V. Dierolf, *Appl. Phys. Lett.*, **99**, 122506 (2011).
50. A. Vallan Bruno Cruz, Prashant P. Shinde, Vijay Kumar, and J. M. Zavada, *Phys. Rev. B*, **85**, 045203 (2012).
51. A. Ney, T. Kammermeier, V. Ney, S. Ye, K. Ollefs, E. Manuel, S. Dhar, K. H. Ploog, E. Arenholz, F. Wilhelm, and A. Rogalev, *Phys. Rev. B*, **77**, 233308 (2008).
52. T. Dietl, *Nat. Mater.*, **9**, 965 (2010).
53. T. Dietl, K. Sato, T. Fukushima, A. Bonanni, M. Jamet, A. Barski, S. Kuroda, M. Tanaka, Pham Nam Hai, and H. Katayama-Yoshida, *Rev. Mod. Phys.*, **87**, 1311 (2015).
54. A. Masago, H. Shinya, T. Fukushima, K. Sato, and H. Katayama-Yoshida, *Phys. Rev. B*, **98**, 214426 (2018).
55. N. Nepal, M. Oliver Luen, J. M. Zavada, S. M. Bedair, P. Frajtag, and N. A. El-Masry, *Appl. Phys. Lett.*, **94**, 132505 (2009).